Modern Physics Letters B
Vol. 36, No. 4 (2022) 2150553 (10 pages)

DOI: 10.1142/S0217984921505539

Theoretical fabrication of subwavelength structures by surface plasmon interference based on complementary grating

Xiangxian Wang*, Yaqian Ren, Tianxu Jia and Yingwen Su
School of Science, Lanzhou University of Technology, Lanzhou 730050, China
**wangxx869@lut.edu.cn*

Yunping Qi
College of Physics and Electronic Engineering, Northwest Normal University, Lanzhou 730070, China
qiyunping@nwnu.edu.cn

Xiaolei Wen
Center for Micro- and Nanoscale Research and Fabrication, University of Science and Technology of China, Hefei 230026, China
xiaolwen@ustc.edu.cn

Received 15 August 2021
Revised 14 October 2021
Accepted 17 October 2021
Published 5 January 2022

This paper presents a surface plasmon interference lithography technique based on the complementary grating, which comprises silicon gratings and complementary aluminum grating masks, for fabricating subwavelength structures. In this theoretical study, the optimal parameters of the complementary grating structure were determined using the reflectance spectrum. The optical field distributions of one- and two-dimensional subwavelength structures were obtained using the finite-difference time-domain method and rotation-related formulas. The results of numerical evaluations show that a one-dimensional periodic structure with a half-pitch resolution of 60.5 nm (approximately $\lambda/6.7$) can be fabricated. In addition, subwavelength structures can be diversified using different rotation methods to expose the photolithography samples, such as square dot arrays and quasi-hexagonal closely packed structures. The proposed method combines surface plasmon interference with sample rotation, thereby enabling fabrication of abundant subwavelength structures.

Keywords: Surface plasmon lithography; complementary grating; periodic pattern.

*Corresponding author.

1. Introduction

The introduction of micro and nanostructures to control the diffraction and propagation of light to realize new optical properties has attracted considerable research attention. An increasing number of studies have reported using micro and nanostructures in different applications, such as filters,[1,2] sensors,[3–6] metadevices,[7,8] and photonic crystals.[9] Lithography is a key process in the fabrication of micro and nanostructures. Because of the diffraction limit,[10–12] that is, the inability of a light beam to be focused onto a space of size that is smaller than half its wavelength, high-density integrated devices cannot meet the manufacturing requirements. New lithography techniques involving electron beams[13] and X-rays[14] have the ability to exceed the diffraction limit and generate subwavelength structures.[15–17] However, these methods increase not only the technical difficulty but also the cost, which is problematic for large-scale nanofabrication. The surface plasmon (SP) resonance phenomenon has a wide range of applications in device fabrication,[18–21] photocatalysis,[22,23] solar absorption,[24–27] functional instrumentation,[28–31] and surface-enhanced Raman scattering.[32,33] Thus, SP lithography,[34–36] which employs the interference effect of SP waves, is proposed for fabrication of periodic subwavelength structures with good application prospects for industrial production.

Luo *et al.*[37] proposed an SP resonant interference lithography technique along with the design and fabrication of a grating structure to excite the SPs; they successfully inscribed a one-dimensional (1D) grating with a period of less than 100 nm. Wang *et al.*[38] optimized the SP structure to not only prevent pollution on the surface of the photoresist but also produce two interference lithography modes between the SPs and guide mode by varying the thickness of the photoresist. In 2020, Liu *et al.*[39] proposed a special plasmonic lithography prototype based on coupling of the bulk plasmon polariton and waveguide modes; they found that subwavelength structures with a feature size of up to $\lambda/8$ could be fabricated for an incident light of wavelength 436 nm.

In this work, we propose the SP interference lithography technique based on a complementary grating using an excitation laser source of wavelength 405 nm. The results of numerical investigations show that a 1D periodic structure with a half-pitch resolution of 60.5 nm (approximately $\lambda/6.7$) can be fabricated theoretically. Furthermore, using different rotation methods to expose the photolithography samples, diversified structures may be fabricated, such as square dot arrays with a period of 121 nm and quasi-hexagonal closely packed structures with a period of 138 nm. In contrast with the aforementioned lithography technique, we emphasize the richness of the two-dimensional (2D) patterns while obtaining 1D periodic subwavelength structures.

2. Theoretical Analysis

Figure 1(a) illustrates the structure of SP interference lithography based on the complementary grating. The complementary grating is composed of silicon (Si) and complementary aluminum (Al) gratings. Fused quartz is used as both the upper and lower substrate materials. In practical lithography applications, Si gratings are evenly arranged on the substrate, and the gaps are filled with Al to constitute the complementary grating structure. The photoresist that is in close contact with the complementary grating is spin coated on the substrate. The XOY plane is defined as the interface between the Al and photoresist, with the Z-direction being perpendicular to the interface and its positive direction pointing toward the Si gratings. Figure 1(b) shows the cross-section of the plasmon lithography with the complementary grating structure, which represents the inscribing of a 1D subwavelength structure without sample rotation.

For the given materials and based on the SP theory, the resonance wavelength for normal incidence, λ_{plasmon}, is expressed as[37]

$$\lambda_{\text{plasmon}} = \Lambda\sqrt{\frac{\varepsilon_m\varepsilon_d}{\varepsilon_m + \varepsilon_d}}, \tag{1}$$

where Λ is the periodicity of the complementary grating and ε_m and ε_d represent the dielectric constants of the metal and surrounding material, respectively.

Based on the aforementioned research, the patterns of the 2D subwavelength structures can be produced in several ways by rotating the photolithography sample through a range of rotation angles with multiple exposures. The optical field

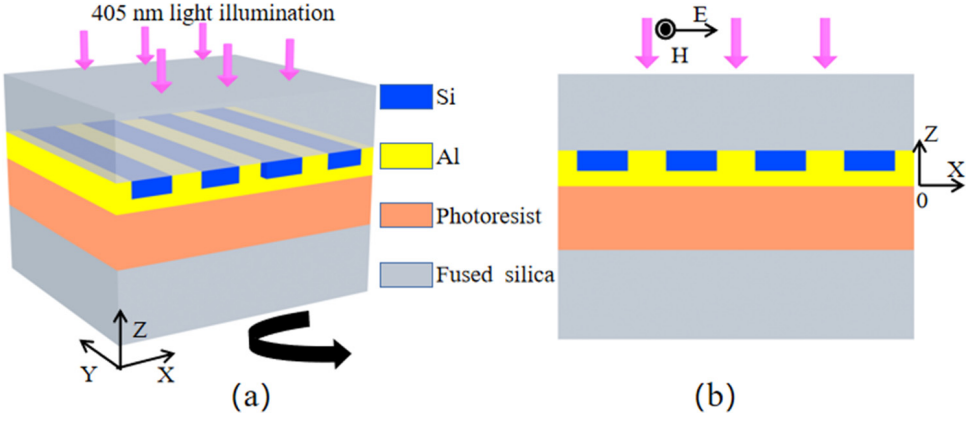

Fig. 1. (Color online) (a) Structure of the SP interference lithography method based on complementary gratings. (b) Cross-section of the plasmon lithography with complementary grating structure.

distribution after exposure for a certain rotation angle is expressed as[40]

$$(X_n, Y_n, Z_n, I_n) = (X, Y, Z, I) \begin{pmatrix} \cos\alpha_n & \sin\alpha_n & 0 & 0 \\ -\sin\alpha_n & \cos\alpha_n & 0 & 0 \\ 0 & 0 & 1 & 0 \\ 0 & 0 & 0 & 1 \end{pmatrix}, \tag{2}$$

where I_n is the optical field intensity after the nth exposure and α_n is the angle by which the sample is rotated. For $N-1$ rotations and N exposures, the resulting total interference field distribution is the superposition of all the interference optical fields, which can be written as

$$I(X, Y, Z) = \sum_{n=1}^{N} I(X_n, Y_n, Z_n, \alpha_n). \tag{3}$$

3. Numerical Simulation Results and Discussion

Because the complementary grating is composed of Si and Al gratings, the periods of the two gratings are identical and filling factor f is complementary; f is defined as the ratio of the metal width to the period. We assume that the monochromatic wave has a wavelength of $\lambda = 405$ nm and that the refractive indexes of the fused quartz and photoresist are 1.4696 and 1.6,[41] respectively. The thickness of the photoresist is 100 nm, and the dielectric constants of Si and Al are $29.450 + 3.7203\mathrm{i}$[42] and $-23.737 + 4.9024\mathrm{i}$,[43] respectively. By considering the Si gratings as the research object, we adopted the finite-difference time-domain method for the numerical analysis to optimize the structure. The reflection spectrum shown in Fig. 2 is modeled by scanning the thickness of the Si grating for a complementary grating thickness of 35 nm. Moreover, the perfectly matched layers condition was applied to the upper and lower substrates where the incident light wavelengths ranged from 200 nm to

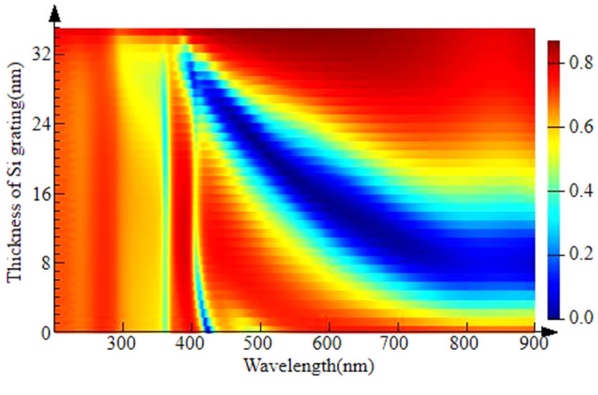

Fig. 2. (Color online) Reflection spectra as a function of the thickness of the Si grating in the complementary grating structure, whose thickness is 35 nm.

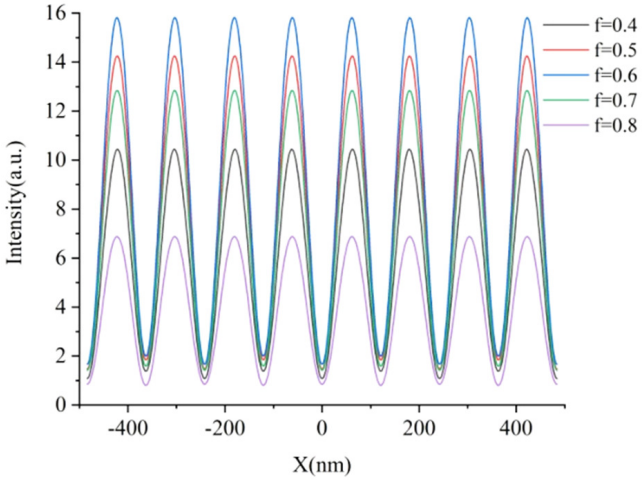

Fig. 3. (Color online) Optical field distributions along the x-axis at $Z = -5$ nm for different fill factor values.

900 nm. As observed, low reflectivity is acquired when the Si grating thickness is approximately 30 nm and incident light wavelength is 405 nm. Nevertheless, the Al film thickness in the surface underlying the complementary grating is only 5 nm if the Si grating thickness is 30 nm. However, as preparing a 5-nm thin film is practically difficult, the thickness of the Si grating was set as 15 nm. The numerical results show that a 1D subwavelength with high contrast can still be produced under these structural conditions. We use only the 405 nm source as the example for numerical simulations in this study. In practical lithography, other wavelengths are also acceptable; however, it would necessitate adjustment of the period and thickness of the complementary grating to determine the optimal solution via the reflection spectrum. In addition, the period and intensity of the obtained interference patterns may change.

The feature size of the fabricated subwavelength structure is independent of the complementary grating fill factor. Variations in the fill factors influence the optical field intensities considerably but have little influence on the contrast. The contrast, γ, is defined as $\gamma = (|I|_{\max} - |I|_{\min})/(|I|_{\max} + |I|_{\min})$, where $|I|_{\max}$ and $|I|_{\min}$ are the maximum and minimum intensities, respectively. Figure 3 shows the optical field distribution along the x-axis at $Z = -5$ nm for different values of the fill factor f. When f increases from 0.4 to 0.8 in increments of 0.1, the contrast remains unchanged at a value of approximately 0.8. In the following numerical calculations, we choose $f = 0.6$ for the relatively higher optical field intensity distribution.

In practical applications, the quality of the lithographic patterns are further evaluated by considering two important requirements, namely field intensity distribution and contrast. Figure 4(a) shows the optical field intensity distribution of SP interference based on the complementary grating structure, which is the result

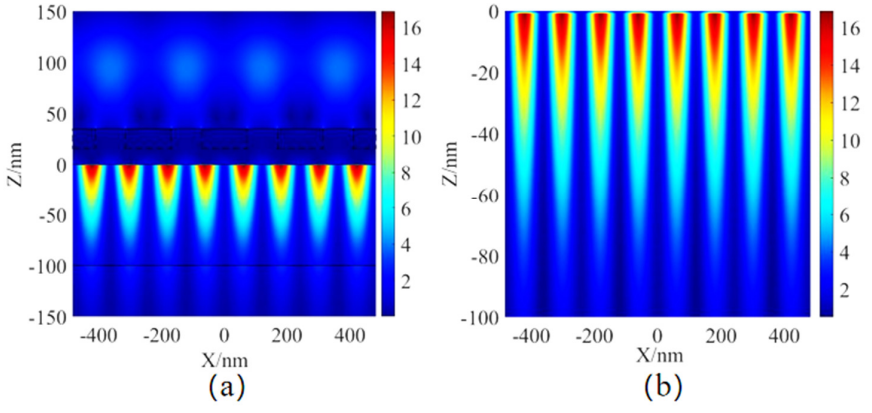

Fig. 4. (Color online) Optical field intensity distributions (a) over the entire structure and (b) in the photoresist layer.

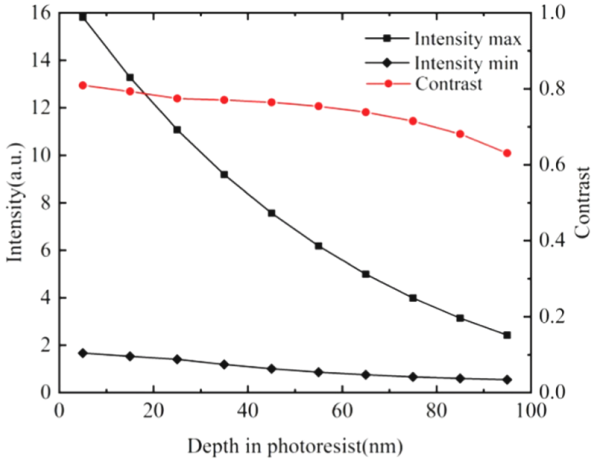

Fig. 5. (Color online) Electric field intensities and contrast values of interference fringes at different depths within the photoresist layer.

of direct exposure of the sample without rotation. It is easily noted that the field enhancement is concentrated mainly near the interface between the photoresist and Al under SP excitations. The spatial resolution is improved significantly since the wavelength of the SP light is shorter than that of the incident light. For convenient analysis of the interference fringes, the field distribution in the photoresist layer is shown in Fig. 4(b), from which a periodic pattern with a half-pitch resolution of 60.5 nm (approximately $\lambda/6.7$) is obtained. The correlations between the extreme intensity values and corresponding contrast at distinct photoresist depths are shown in Fig. 5. The photoresist depths were varied from 5 nm to 95 nm in increments of 10 nm; the contrast values for the interference fringes were calculated using the

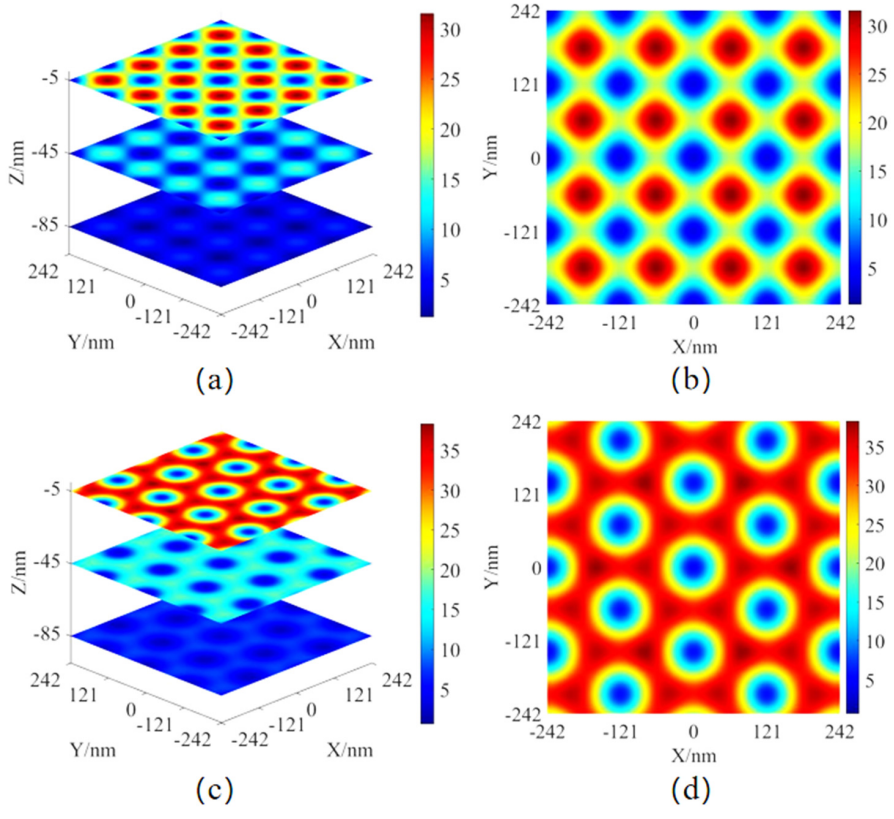

Fig. 6. (Color online) Slice maps of the optical field intensity distributions at $Z = -85$, -45 and -5 nm for (a) 90° and (c) 60° rotations. The cross-sectional field distributions at $Z = -5$ nm are shown for rotation angles of (b) 90° and (d) 60°.

contrast formula noted above. Notably, the contrast decreases slowly throughout the photoresist layer, and high electric field intensity and contrast can increase the lithography efficiency, especially its exposure stability.

Based on discussion of the SP lithography of a 1D grating, various 2D subwavelength patterns can be obtained if different rotation methods are used to rotate and expose the lithographic samples. For example, a 2D periodic subwavelength structure can be fabricated theoretically using different rotation angles on the photolithography sample with multiple exposures. Figure 6(a) shows the resulting optical field intensity distribution of the photoresist at cross-sections with $Z = -85$, -45 and -5 nm when the sample is rotated through 90° and re-exposed. This distribution indicates that the electric field intensities of the SPs decay exponentially in the Z-direction. Figure 6(b) shows the field distribution at the cross-section with $Z = -5$ nm. The pattern comprising two square regions with different intensities is a 2D square dot array with a period of 121 nm. According to the contrast formula, the field intensities $|I|_{\max}$ and $|I|_{\min}$ are 31.555 and 1.2, respectively, such

the contrast is 0.93. Similarly, Fig. 6(c) displays the results of the sample being rotated twice at an angle of 60° each, with three exposures after each rotation. The resulting electric field distribution at $Z = -5$ nm is shown in Fig. 6(d). Owing to the small value of $|I|_{\min}$, the corresponding contrast is 0.97, which is slightly different from that in Fig. 6(b). Figure 6(d) shows that a bow pattern consisting of two equilateral triangles with a common vertex was obtained using a negative photoresist. Since the contrast is higher than 0.2, patterns can also be produced for negative photoresist; hence, the negative photoresist is generally chosen. However, the contrast of the 2D pattern shown here is theoretically higher than 0.9, such that the corresponding patterns can be fabricated using either the negative or positive photoresist. Thus, quasi-hexagonal closely packed structures with uniform intensity distributions within the quasi-hexagons and a period of 138 nm are obtained using a positive photoresist.

In addition to 60° and 90°, the sample rotation angles can be set to 30° and 45°, which produce 2D structures with different periods. The selected sample rotation angle should, however, meet the requirement that it is a common divisor of 180°. Moreover, the sample rotation angle decreases with increase in rotation as well as exposure time.

4. Conclusion

This paper presents a SP interference lithography technique based on complementary gratings. Numerical simulations were performed to show that 1D periodic subwavelength structures could be theoretically produced with a half-period of 60.5 nm ($\lambda/6.7$). In addition, multiple 2D subwavelength structures, such as a square dot array with a period of 121 nm and quasi-hexagonal closely packed structure with a period of 138 nm, could be obtained by varying the rotation angles and exposure times. This method provides advantages such as a simple structure, high resolution, and diversified patterns for the subwavelength structures. The proposed lithography method combines SP interference with sample rotations, thereby enabling potential applications for the development of abundant subwavelength structures. In addition, it has strong prospects for use within industrial manufacturing.

Acknowledgments

This work was supported by the National Natural Science Foundation of China (NSFC) [Grant No. 61865008] and the HongLiu First-Class Disciplines Development Program of Lanzhou University of Technology.

References

1. Y. P. Qi, P. Y. Zhou, T. Zhang, X. W. Zhang, Y. Wang, C. Q. Liu, Y. L. Bai and X. X. Wang, *Results Phys.* **14** (2019) 102506.
2. Y. P. Qi, X. W. Zhang, P. Y. Zhou, B. B. Hu and X. X. Wang, *Acta Phys. Sin.* **67** (2018) 197301.

3. C. Liu, J. W. Wang, F. M. Wang, W. Q. Su, L. Yang, J. W. Lv, G. L. Fu, X. L. Li, Q. Liu, T. Sun and P. K. Chu, *Opt. Commun.* **464** (2020) 125496.
4. X. X. Wang, J. K. Zhu, Y. Q. Xu, Y. P. Qi, L. P. Zhang, H. Yang and Z. Yi, *Chin. Phys. B* **30**(2) (2021) 024207.
5. J. Chen, H. Nie, C. Peng, S. B. Qi, C. J. Tang, Y. Zhang, L. H. Wang and G. S. Park, *J. Lightwave Technol.* **36**(16) (2018) 3481.
6. J. Qian, J. M. Li, J. F. Zhi and S. D. Qin, *Chin. J. Anal. Chem.* **41**(5) (2013) 738.
7. N. I. Zheludev and Y. S. Kivshar, *Nat. Mater.* **11**(11) (2012) 917.
8. S. Y. Xiao, T. Wang, T. T. Liu, C. B. Zhou, X. Y. Jiang and J. F. Zhang, *J. Phys. D: Appl. Phys.* **53**(50) (2020) 503002.
9. M. Miyake, Y. Chen, P. V. Braun and P. Wiltzius, *Adv. Mater.* **21**(29) (2009) 3012.
10. D. K. Gramotnev and S. I. Bozhevolnyi, *Nat. Photonics* **4**(2) (2010) 83.
11. M. M. Alkaisi, R. J. Blaikie, S. J. McNab, R. Cheung and D. R. S. Cumming, *Appl. Phys. Lett.* **75**(22) (1999) 3560.
12. J. J. Dong, J. Liu, G. G. Kang, J. H. Xie and Y. T. Wang, *Sci. Rep.* **4**(1) (2014) 5618.
13. Y. F. Chen, *Microelectron. Eng.* **135** (2015) 57.
14. N. Mojarad, D. Fan, J. Gobrecht and Y. Ekinci, *Opt. Lett.* **39**(8) (2014) 2286.
15. K. V. Sreekanth, J. K. Chua and V. M. Murukeshan, *Appl. Opt.* **49**(35) (2010) 6710.
16. G. F. Liang, C. T. Wang, Z. Y. Zhao, Y. Q. Wang, N. Yao, P. Guo, Y. F. Luo, G. H. Gao, Q. Zhao and X. G. Luo, *Adv. Opt. Mater.* **3**(9) (2015) 1248.
17. K. V. Sreekanth and V. M. Murukeshan, *J. Micro/Nanolithogr. MEMS, MOEMS* **9**(2) (2010) 023007.
18. X. X. Wang, J. K. Zhu, H. Tong, X. D. Yang, X. X. Wu, Z. Y. Pang, H. Yang and Y. P. Qi, *Chin. Phys. B* **28**(4) (2019) 044201.
19. J. W. Wang, C. Liu, F. M. Wang, W. Q. Su, L. Yang, J. W. Lv, G. L. Fu, X. L. Li, Q. Liu, T. Sun and P. K. Chu, *Results Phys.* **18** (2020) 103240.
20. T. X. Jia, X. X. Wang, Y. Q. Ren, Y. W. Su, L. P. Zhang, H. Yang, Y. P. Qi and W. M. Liu, *Coatings* **11**(1) (2021) 62.
21. Z. D. Yan, X. Lu, W. Du, Z. Q. Lv, C. J. Tang, P. G. Cai, P. Gu, J. Chen and Z. Yu, *Nanotechnology* **32**(46) (2021) 465202.
22. S. T. Guan, R. S. Li, X. F. Sun, T. Xian and H. Yang, *Mater. Technol.* **36**(10) (2020) 603.
23. Y. P. Wang, X. F. Sun, T. Xian, G. R. Liu and H. Yang, *Opt. Mater.* **113** (2021) 110853.
24. G. Q. Liu, J. Chen, P. P. Pan and Z. Q. Liu, *IEEE J. Sel. Top. Quantum Electron.* **25**(3) (2018) 4600507.
25. Z. H. Chen, H. Chen, H. G. Jile, D. Y. Xu, Z. Yi, Y. L. Lei, X. F. Chen, Z. G. Zhou, S. S. Cai and G. F. Li, *Diam. Relat. Mater.* **115** (2021) 108374.
26. Y. Q. Wang, Y. T. Yi, D. Y. Xu, Z. Yi, Z. Y. Li, X. F. Chen, H. G. Jile, J. G. Zhang, L. C. Zeng and G. F. Li, *Physica E* **131** (2021) 114750.
27. F. Q. Zhou, F. Qin, Z. Yi, W. T. Yao, Z. M. Liu, X. W. Wu and P. H. Wu, *Phys. Chem. Chem. Phys.* **23**(31) (2021) 17041.
28. Y. Deng, G. G. Cao, H. Yang, X. Q. Zhou and Y. W. Wu, *Plasmonics* **13**(1) (2018) 345.
29. L. Y. Jiang, Y. T. Yi, Y. J. Tang, Z. Y. Li, Z. Yi, L. Liu, X. F. Chen, R. H. Jian, P. H. Wu and P. G. Yan, *Chin. Phys. B* **31**(3) (2022) 038101.
30. G. T. Cao, H. J. Li, Y. Deng, S. P. Zhan, Z. H. He and B. X. Li, *Plasmonics* **9**(5) (2014) 1163.
31. Y. Deng, G. G. Cao, Y. W. Wu, X. Q. Zhou and W. H. Liao, *Plasmonics* **10**(6) (2015) 1537.

32. Y. Wu, X. X. Wang, X. L. Wen, J. K. Zhu, X. L. Bai, T. X. Jia, H. Yang, L. P. Zhang and Y. P. Qi, *Phys. Lett. A* **384** (2020) 126544.
33. X. X. Wang, Y. Wu, X. L. Wen, J. K. Zhu, X. L. Bai, Y. P. Qi and H. Yang, *Opt. Quantum Electron.* **52**(5) (2020) 238.
34. K. V. Sreekanth, V. M. Murukeshan and J. K. Chua, *Appl. Phys. Lett.* **93**(9) (2008) 093103.
35. L. Q. Liu, Y. F. Luo, Z. Y. Zhao, W. Zhang, G. H. Gao, B. Zeng, C. T. Wang and X. G. Luo, *Sci. Rep.* **6**(1) (2016) 30450.
36. X. Chen, F. Yang, C. Zhang, J. Zhou and L. J. Guo, *ACS Nano* **10**(4) (2016) 4039.
37. X. G. Luo and T. Ishihara, *Appl. Phys. Lett.* **84**(23) (2004) 4780.
38. X. X. Wang, D. G. Zhang, Y. K. Chen, L. F. Zhu, W. H. Yu, P. Wang, P. J. Yao, H. Ming, W. X. Wu and Q. J. Zhang, *Appl. Phys. Lett.* **102** (2013) 031103.
39. H. C. Liu, W. J. Kong, Q. G. Zhu, Y. Zheng, K. S. Shen, J. Zhang and H. Lu, *J. Phys. D*: *Appl. Phys.* **53**(13) (2019) 135103.
40. X. W. Guo, Q. M. Dong, R. Y. Shi, S. H. Li and J. L. Du, *Microelectron. Eng.* **105** (2013) 103.
41. X. X. Wang, Z. Y. Pang, H. Tong, X. X. Wu, X. L. Bai, H. Yang, X. L. Wen and Y. P. Qi, *Results Phys.* **12** (2019) 732.
42. D. E. Aspnes and A. A. Studna, *Phys. Rev. B* **27**(2) (1983) 985.
43. A. D. Rakić, *Appl. Opt.* **34**(22) (1995) 4755.